

Session MP-4

Materials/Processes(4)

Low Temperature Direct Cu-Cu Bonding with Low Energy Ion Activation Method

T. H. KIM, M. M. R. HOWLADER, T. ITOH, T. SUGA, The University of Tokyo, Japan

Molding 3-DOF Planar Positioning and Orientation Tables with Large-Deflective Polymer Hinges and Links for Packaging Manufacturing Systems

Mikio HORIE, Shuusaku KUBO, Daiki KAMIYA, Tokyo Institute of Technology, Japan

Adhesion of RF Bias-Sputtered Cr Thin Films onto Photosensitive Polyimide Substrates

Sun Young KIM, Young-Ho KIM, C. S. Yoon, Hanyang University, Korea

Low Temperature Direct Cu-Cu Bonding with Low Energy Ion Activation Method

T. H. Kim, M. M. R. Howlader, T. Itoh, and T. Suga
Research Center for Advanced Science and Technology (RCAST),
The University of Tokyo, Komaba 4-6-1, Meguro-ku, Tokyo 153-8904 Japan
Phone:+81-03-5452-5180 Fax:+81-03-5452-5184 E-mail:kim@su.rcast.u-tokyo.ac.jp

Abstract

This paper describes a copper wafer bonding for the application of three-dimensional integration and wafer-level packaging. Cu-Cu direct bonding at low temperature using low energy ion activation method was investigated. 8-inch silicon wafers were coated with 80 nm copper and the copper surfaces were cleaned by irradiation of 50-100 eV argon ion beam before mating them together. The cleaned surfaces were examined by Auger electron spectroscopy (AES). It was observed that carbon contaminations and native oxide layer on the copper surface were effectively removed by 1 min ion beam irradiation without any wet cleaning process. After cleaning the surfaces, two wafers were brought into contact and pressed up to 1000 kgf in the bonding chamber at ultra high vacuum (UHV) pressure. The surfaces were examined by atomic force microscope (AFM) and the bonded interface was investigated by tensile tests. Details of characterization of bonding interface of Cu-Cu and the effects of low energy ion beam on the bonding will be described.

Introduction

Cu-Cu bonding has been of great interest in recent years because it is imperative in interconnection technology for three dimensional packaging of microelectronics [1-2]. Copper is the most popular and promising material for wafer metallization since it has good electrical conductivity. For this reason, copper wafer bonding technology is a key issue to realize a wafer level packaging with low signal delay and high performance.

In order to realize the copper interconnection for practical applications in industry, copper bonding should be performed at low temperature. If copper is heated at high temperature, it will diffuse into other devices on a wafer resulting in degradation of their function [3]. But chemically treated copper needs high temperature annealing to increase bonding strength. To reduce the annealing temperature, the surface activated bonding (SAB) process may be used. SAB is a process that joins dissimilar materials due to the adhesion force between atoms of two atomically clean surfaces in an ultra high vacuum (UHV) at room temperature [4-5]. The highly accelerated fast argon atom beam (FAB) physically bombards contaminants and oxides on the wafer surface resulting in removing them. By removing the contaminants and oxides, the activated clean surfaces can be obtained for direct bonding at low temperature. SAB has been used to bond many kinds of material without adhesives at room temperature. The atomically clean copper surface can be obtained using FAB without any wet chemical cleaning process. However, some damage on its surface due to the bombardment of energetic particles can be induced during FAB process. The

damage may degrade the resulting bonding interface quality and the performance of devices fabricated on a wafer. To avoid this, the acceleration voltage should be lowered and activation process time should be shortened.

In this work, low energy Ar ion beam was used to activate copper surface. By low energy Ar ion beam activation for short time, the 8 inch Si wafers coated with copper were successfully bonded at room temperature without any adhesive materials. Tensile test results show the surface energy of the bonded samples is sufficiently high for actual applications in industry.

Experimental

8 inch p-Si(100) coated with SiO₂/SiN/TaN/Ta/Cu by sputtering was used in the work. The thickness of Cu is 80 nm and total thickness of the thin films deposited on Si wafer is 192 nm. The SAB machine consists of chambers for ion beam processing, surface analyzing (Auger electron spectroscopy), heating, turning over, preliminary bonding, and bonding chamber as shown in Fig. 1. Two wafers are loaded in the load lock chamber and transported to the process chamber. The wafer surface was activated by Ar ion beam bombardment in the process chamber. The operation parameters are given in Table I. One of the surface activated wafers is transferred to the turning over chamber and turned over. Prior to pressing in the bonding chamber, two wafers are pre-bonded to give initial bonding by the load of 50 kgf in the pre-bonding chamber. After pre-bonding, the mated wafer pair is pressed up to 1000 kgf by the roller in the bonding chamber. The roller pressing range is limited up to ± 5 cm from the wafer center to avoid wafer breakage during pressing process.

The bonded wafer pair was diced into 10×10 mm² pieces to perform tensile tests for measuring the bonding energy. The sample pieces were glued to metal bars for setting them to tensile machine and debonded.

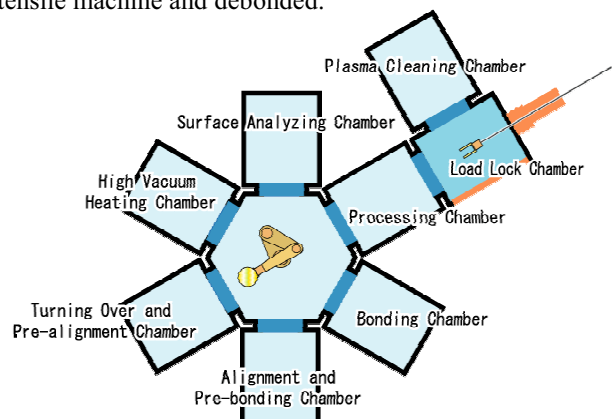


Fig. 1. Schematic diagram of the wafer-scale SAB machine.

Table I. Ion beam process condition for wafers.

Ion gun parameters	
Ar gas flow rate	3 sccm
Acceleration voltage	80 V
Ion beam current	2.92 A
Ion beam irradiation time	1 min
Incidence angle of ion beam	90 degree
Ion energy	50-100 eV

Results and Discussion

Fig. 2. shows the results of AES analysis just before and after 1 min Ar beam process. As shown in the picture, strong peaks of carbon and oxygen are observed before Ar ion beam treatment. However, the peaks are almost removed after Ar ion beam treatment for 1 min. This means that the copper surface is sufficiently clean and activated for direct bonding. It takes about 10 min to finish AES analysis after Ar ion beam treatment. During that time, the copper surface may be re-oxidized due to residual gases (O_2 , H_2O) in the chamber although the chambers keep UHV condition. But AES results show that re-oxidation of cleaned surface during analysis and of transportation wafers is not so critical. It is obvious that a short exposure to low energy ion beam makes the copper surface clean and activated it without heating or wet chemical cleaning process. The oxygen and carbon level on copper surface becomes lower than the limits of detectability by AES.

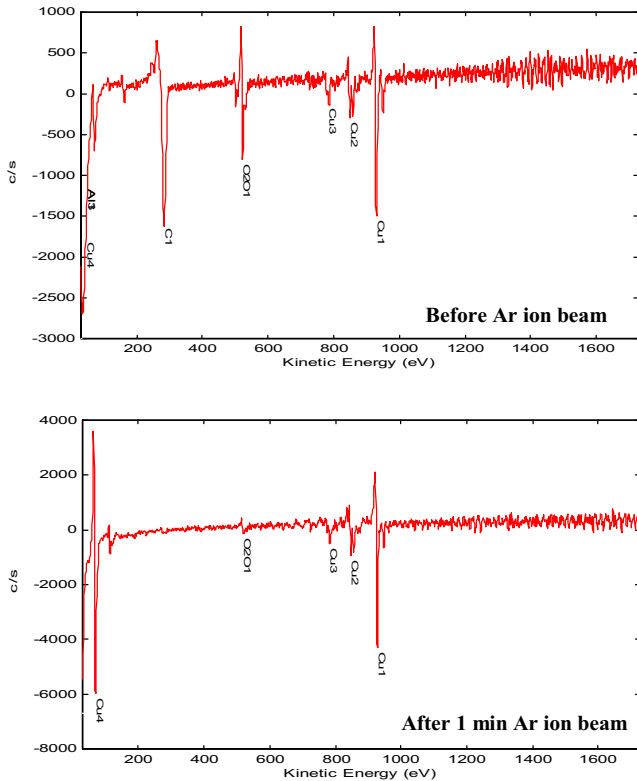


Fig. 2. AES spectra of copper surface just before and after Ar ion beam process.

The atomic force microscope (AFM) images of the copper surface before and after Ar ion beam process are shown in Fig. 3. The image was taken immediately after Ar ion beam treatment. The AFM results reveal that 1 min Ar ion beam treatment does not affect the roughness of copper surface. This means that the short time and low energy ion beam treatment can activate the copper surface without degradation of its surface. This property characterized by low damage may guarantee that high quality bonding without degradation of device performance and bonded interface will be realized for practical applications in industry.

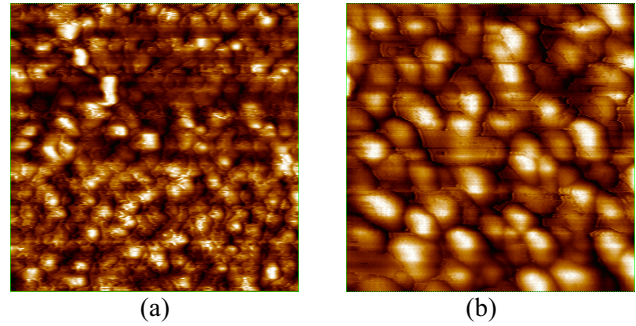


Fig. 3. AFM scan over copper surface (a) before Ar ion beam treatment, rms(3.42nm); (b) after Ar ion beam treatment for 1 min. rms (3.39nm). Scan area is $1 \times 1 \mu m^2$.

To increase bond strength, the wafer pair was pressed by the roller. The wafer pair is not fully pressed over whole area but partly pressed. The map of bonded sample dices is shown in Fig. 4. The dices filled with black were tested by the tensile machine.

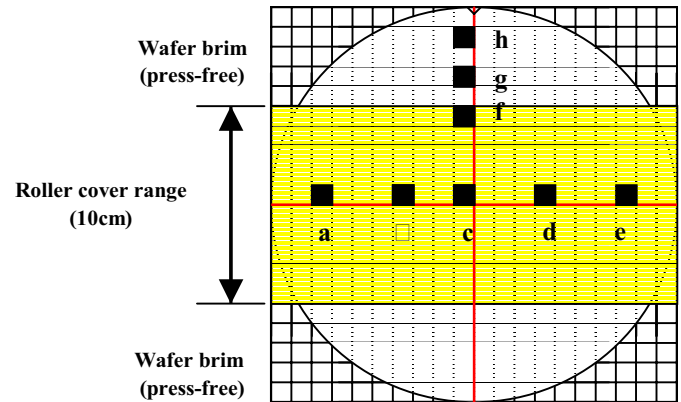


Fig. 4. The map of diced wafer for tensile tests: The bonded pair consists of two parts. One is a directly pressed part by the roller and the other is a press-free part. Samples of a-f are directly pressed by the roller but samples of g, h are not.

The wafers pair was tightly bonded together over whole wafer area. The bonding energy was so strong that it was impossible to debond the interface of samples. Some of the samples were fractured from the bulk material and the others were fractured from the glue. The glue could not mechanically withstand external tensile stress resulting in breaking up during the test. The glue could withstand up to 647 N. This means that the surface energy is higher than 6.47 MPa at least.

The dices in the wafer brim also showed the three dimensional fracture. The brim of the wafer pair can not be mechanically pressed with high load although the roller gives a lot of weigh on the center of the wafer pair. But the results of tensile test show that the bonding strength is sufficiently high. This means that the bonding strength is not so sensitive to the load of press. The bonding energy of dices is very high everywhere on the wafer. This feature enables the wafer pair to be bonded with much reduced load which is advantageous to wafers having mechanically brittle devices on it. Fig. 5. shows the debonded samples in the wafer brim. Samples were fractured from the bulk material. As shown in Fig. 5., some part of the sample h is fractured from the copper surface but other part from the bulk. All samples were fractured fully from the bulk or glue like the sample f in Fig. 5. except the sample h.

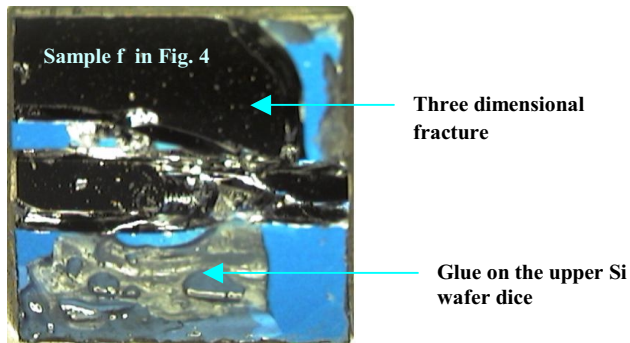
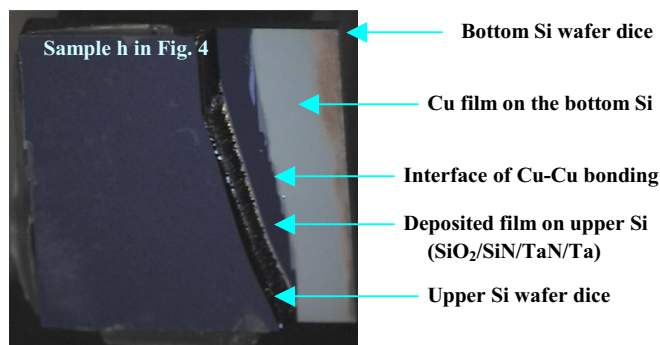


Fig. 5. Bulk fracture pattern of the bonded sample in the brim of the wafer pair.

It took 30 minutes to perform Ar beam treatment, turning over, pre-bonding, and final bonding of two wafers in the bonding chamber in an UHV ($\sim 10^{-8}$ torr). The bonding result shows that exposing clean copper surface to vacuum of $\sim 10^{-8}$ torr for 30 min does not affect the Cu-Cu bonding. As mentioned above, the copper surface having the newly deposited on it during wafer transportation due to residual oxygen and wafer in the chamber is as sensitive to degrading the bonding.

Conclusions

SAB using low energy Ar ion beam has been applied for the bonding of 8 inch Si wafers coated with copper at room temperature. Carbon and oxides on the copper were

effectively removed by the ion beam treatment for 1 minute. AFM analysis shows that low ions beam treatment does not affect the surface roughness. Tensile test results show that the strong Cu-Cu bonding interface equivalent to bulk material is obtained.

Acknowledgments

This work was financially supported by the SRPA (Scientific Research of Priority Areas).

References

1. A. Fan, A. Rahman, and R. Reif, "Copper Wafer Bonding", *Electrochem. and Solid State Lett.* Vol. 2, No. 10 (1999), pp. 534-536
2. A. Fan and R. Reif, "Three-dimensional integration with copper wafer bonding", *Proc. Electrochem. Soc.* Vol. 2001-2 (2001), pp. 124-132.
3. R. S. Muller and T. I. Kamins, *Device Electronics for Integrated Circuit*, 2nd ed. (John Wiley & Sons, New York), 1986, pp. 1-56.
4. H. Takagi, K. Kikuchi, T. R. Chung, and T. Suga, "Surface activated bonding of silicon wafers at room temperature", *Appl. Phys. Lett.*, Vol. 68 (1996), pp. 2222.
5. H. Takagi, R. Maeda, T. R. N. Hosoda, and T. Suga, "Effect of surface roughness on room temperature wafer bonding by Ar beam surface activation", *Jpn. J. Appl. Phys.*, Vol. 38 (1999), pp. 1589.

Molding 3-DOF Planar Positioning and Orientation Tables with Large-Deflective Polymer Hinges and Links for Packaging Manufacturing Systems

Mikio HORIE*, Shuusaku KUBO**, and Daiki KAMIYA*

*;Tokyo Institute of Technology (Precision and Intelligence Laboratory)

**;Graduate Student, Tokyo Institute of Technology

4259, Nagatsuta-cho, Midori-ku, Yokohama, 226-8503, Japan

E-Mail: mhorie@pi.titech.ac.jp, Phone&Fax.:+81-45-924-5048

Abstract

In the former paper(EMAP2000), one of the author has already proposed and developed the molding pantograph mechanism with large-deflective hinges and links for miniature surface mount system for packaging manufacturing system. The characteristic of the pantograph mechanism is investigated theoretically and experimentally. The aimed final miniature manufacturing system for micro assembling is composed of the pantograph mechanisms and the following positioning-and-orientation table.

In this paper, a new molding 3-DOF planar positioning-and-orientation table with large-deflective polymer hinges and links is proposed. The table has two function: a transmission function between manufacturing stations and a positioning-and-orientation function at the manufacturing station. The table with six large-deflective hinges and seven links is made by the small molding injection machine. The used material is PP (Polypropylene). The table has three linear actuators. In the experiments, the singular points of the table mechanism is investigated in its working space and compared with the theoretical results. The performance concerning the transmissibility of the proposed new molding 3-DOF planar positioning-and-orientation table is confirmed.

1. Introduction

Personal information communication on the earth, which human beings have been dreaming of for a long time, has currently come true by the invention of cellular phones. These cellular phones are still becoming miniaturized and light-weighted day by day, and not only cellular phones but also AV devices, computers and their accessories are advancing in the same way. In order to make it easy to bring these to a realization, one of the authors here has already suggested a manipulator system for a portable surface mounting system used for electric devices⁽¹⁾. This study suggests 3-DOF planar positioning-orientation tables molded with links and large-deflective hinges, making it possible to do minute work, since these tables have a function of a conveyance between working stations on the surface mounting direct working lines, as well as a positioning-orientation function in each working station. These tables are created as a model and used to experimentally examine the existing space of singular points of the mechanism composed of hinges. Then, the results are examined and compared with theoretical results to confirm the effectiveness of the suggested mechanism by examining the transmission index of the suggested mechanism composed of hinges.

2. Suggestion on 3-DOF planar positioning-orientation tables composed of large-deflective hinges and links

The subjects in this study are 3-DOF planar positioning-orientation tables composed of large-deflective hinges and links. First, from the result of the examination of the degrees of freedom (DOF) of the mechanism composed of hinges, this study suggests the subjects, 3-DOF planar positioning-orientation tables molded with large-deflective hinges, which are input by three linear actuators in the same direction. Figure 1 shows the entire portable surface mounting systems, and the positioning-orientation tables suggested here are shown at the bottom right-hand corner of the Table. These linear actuators are made to move on two rails, which indicate that they have a function of conveyance between working stations as well as a positioning-orientation function in each working station.

3. Direct / inverse kinematics of 3-DOF positioning tables

Since the subject mechanism used is composed of hinges, the moment occurring at the hinge parts should be taken into consideration. Therefore, focusing on the balance between the entire mechanism and the moment, this study indicates the solution methods for direct kinetic and inverse kinetic problems. Figures 2 and 3 show the results of direct and inverse kinematics of the mechanisms. Moreover, the locus analysis of the mechanism used is simulated, which makes it possible to analyze transmission indexes of the mechanism as well as to analyze kinematics of positioning-orientation tables, which is necessary for designing mechanisms. The mechanism parameters of positioning tables are shown in Fig. 4.

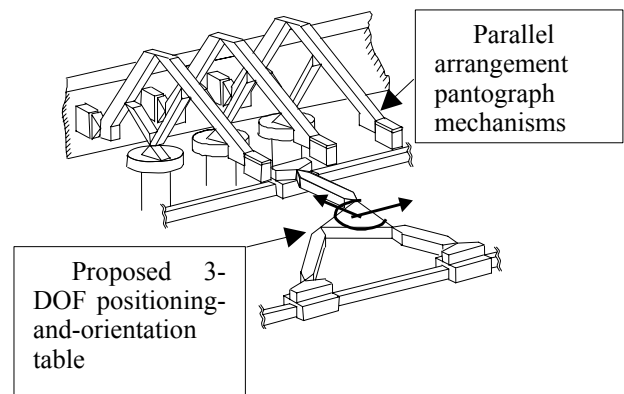


Fig. 1 Proposed 3-DOF positioning-and-orientation table and former proposed parallel arrangement pantograph mechanisms

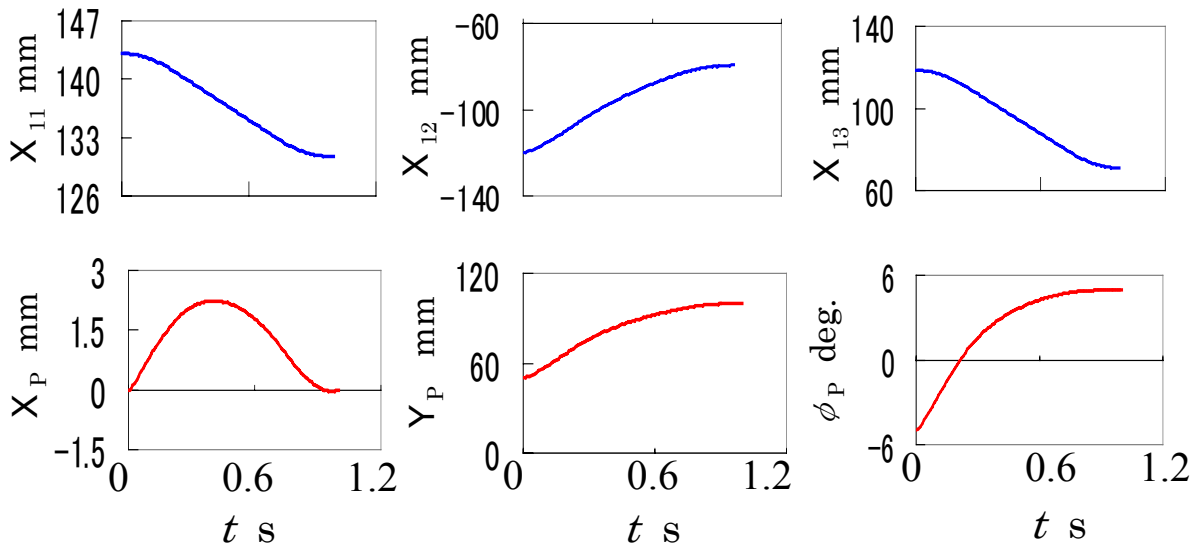


Fig. 2 Results of direct kinematics [From (X_{11}, X_{12}, X_{13}) to (X_p, Y_p, ϕ_p)]

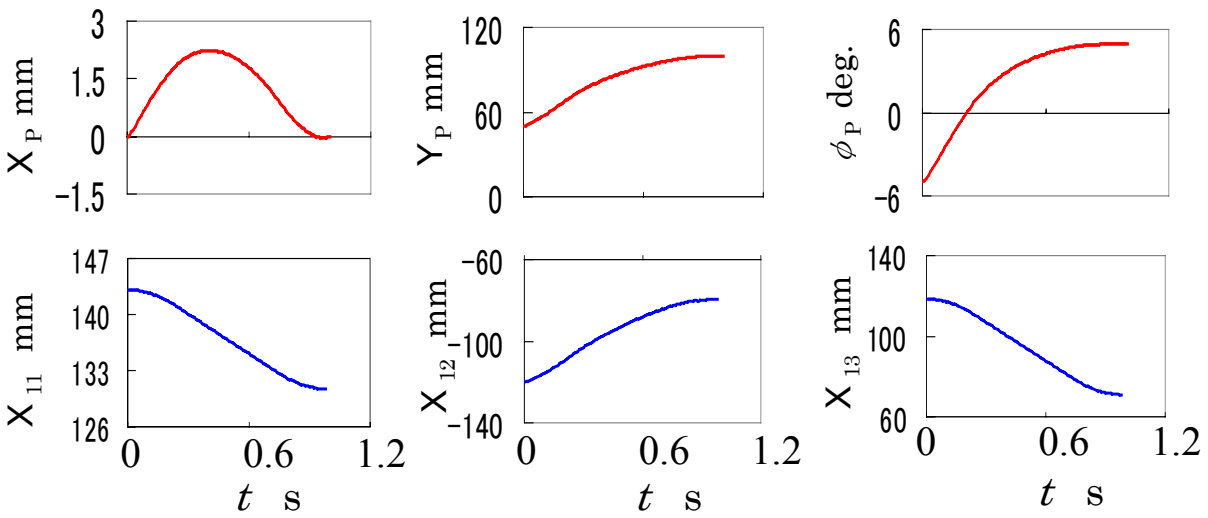


Fig. 3 Results of direct kinematics [From (X_p, Y_p, ϕ_p) to (X_{11}, X_{12}, X_{13})]

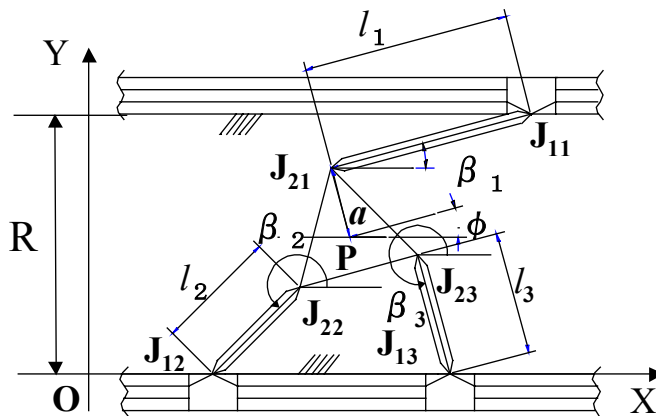


Fig. 4 Parameters of proposed 3-DOF positioning-and-orientation table

4. Transmission indexes of 3-DOF positioning-orientation tables

The transmission index (TI), which is an index for judging the easiness of movement, used to be applicable for only revolute pairs such as ball bearings, which act only by force but do not cause the moment. Equation (1) shows the relationship between TI and a pressure angle in case of 4-bar linkage with revolute pairs shown in Fig.5 (a). Equation (2) shows one in case of the 3-DOF parallel mechanism in Fig.5 (b). In Fig.5 (b), the pressure angle α_2 and α_3 at pairs J_{22} and J_{23} respectively are not drawn.

$$TI = \frac{r}{r_{\max}} = \cos \alpha \quad \dots \dots (1)$$

$$TI = \min. (|\cos \alpha_1|, |\cos \alpha_2|, |\cos \alpha_3|) \quad \dots \dots (2)$$

However, in case of the mechanisms with hinges, it is necessary to consider the effect of moments acting to the hinges. Obtaining this transmission index by the new direction of the force acting on each hinge with consideration of effect of moments acting to the hinges shown Fig.6 (b), this study indicated a method applicable for mechanisms even using

hinges. Figure 6 (a) shows the forces and moments acting to the hinges of output link. In the case where only new forces are considered, the pressure angle is determined by Eq. (3).

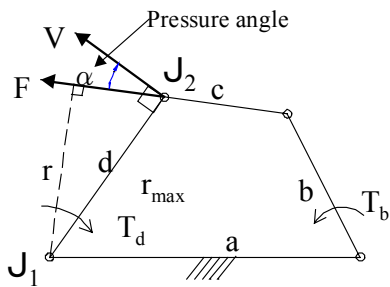
$$\alpha_i = \cos^{-1} \left[\frac{\vec{v}_{2i} \cdot \vec{F}'_{2i}}{|\vec{v}_{2i}| \cdot |\vec{F}'_{2i}|} \right] \quad \dots \dots (3)$$

By use of Eq. (2) and Eq. (3), the singular points are examined theoretically. Figure 7 (a) and 7 (b) show TI distribution in case of the mechanism with revolute pairs and the mechanism with hinges respectively. Then, new forces $F'_{2i} (i=1\sim3)$ are discussed. In Fig. 8, the force components f_1 and F_{21} of F'_{21} in $F_{2i} (i=1\sim3)$ are shown. The difference force f between forces F' and F is given in Eq. (4).

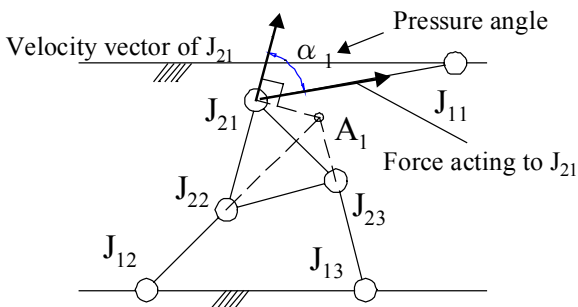
$$f = F' - F \quad \dots \dots (4)$$

where, F : Forces in case of revolute pairs, F' : Forces in case of hinges. The ratio between f and F is given in Eq. (5).

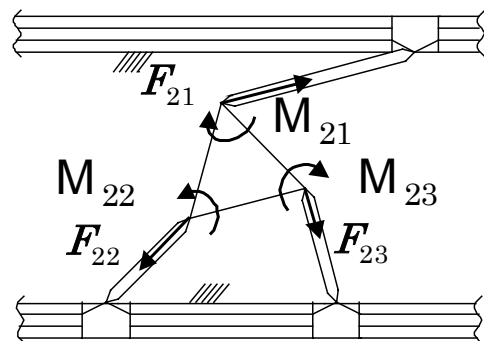
$$|f| : |F| = 1 : k \quad \dots \dots (5)$$



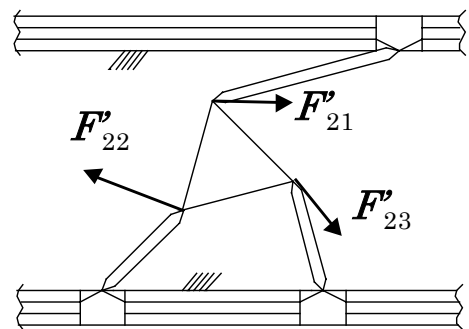
(a) Pressure angle of 4-bar linkage



(b) One pressure angle of 3-DOF parallel mechanism



(a) Forces and moments acting to hinges of output link

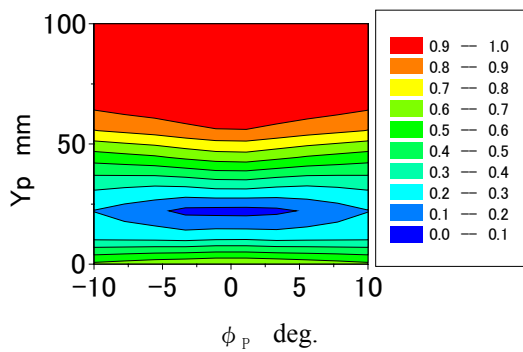


(b) New force directions with consideration of the effect of moments

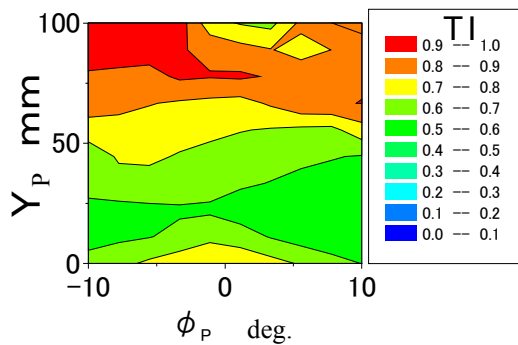
Fig. 6 Forces and moments in 3-DOF parallel manipulator

Fig. 5 Pressure angles of 4 bar linkage and 3-DOF parallel mechanism

Figure 9 shows the result of TI when the parameter k is varied in Eq. (5). Figure 9 (c) is similar with Fig. 7 (a). This result shows that the effects of moments at hinges are small in Fig. 9 (c). From Fig. 9, the effects of moments at hinges are clarified versus k . In the results, we clarified that the mechanism using hinges would cause some changes on its transmission index.

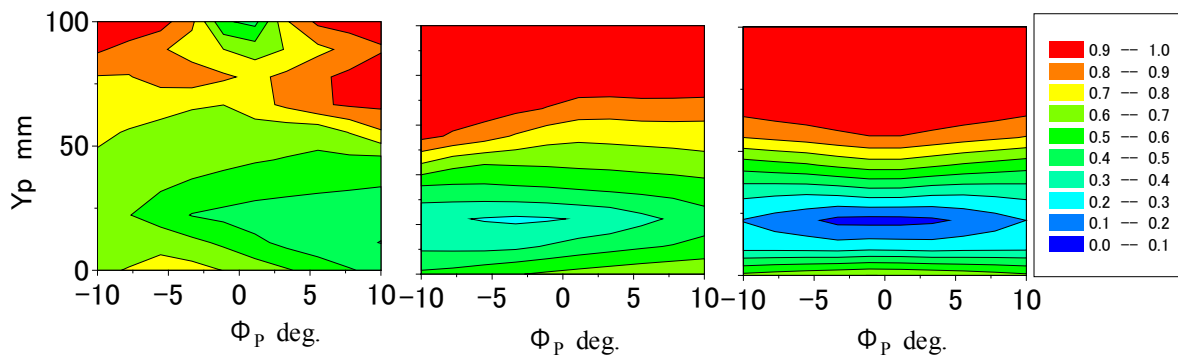


(a) Mechanism with revolute pairs



(b) Mechanism with hinges

Fig. 7 Transmission Index(TI) of 3-DOF positioning-and-orientation mechanism



(a) $k=1$

(b) $k=100$

(c) $k=10000$

Fig. 9 TI distribution versus k

5. Manufacturing a trial model of 3-DOF planar positioning-orientation table and experiments

In addition to the examination of the relationship between the mechanism size and transmission index according to the working space, the method for determining the shape size of positioning tables was clarified using the design flowchart shown in Fig. 10. In order to realize an ideal mechanism, which can satisfy the work space, has a favorite transmissibility, and also has a small shape size. Table 1 shows the specification of table parameters of the design method, while Table 2 shows the design result when the length of three links are determined as design variables.

This study noted the method for manufacturing a trial model by a small injection-molding machine, using polypropylene as a material for this model. Then the suggested positioning table with parameters shown in Table 1 and 2 was actually manufactured and clarified the following important points for manufacturing in order: materials, injection temperatures, and the manufacturing process. Figure 11 shows the positioning-orientation table manufactured by a small

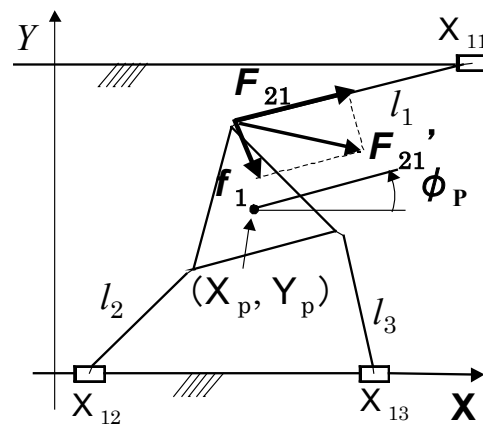


Fig. 8 Force components f_1 and F_{21} of F'_{21}

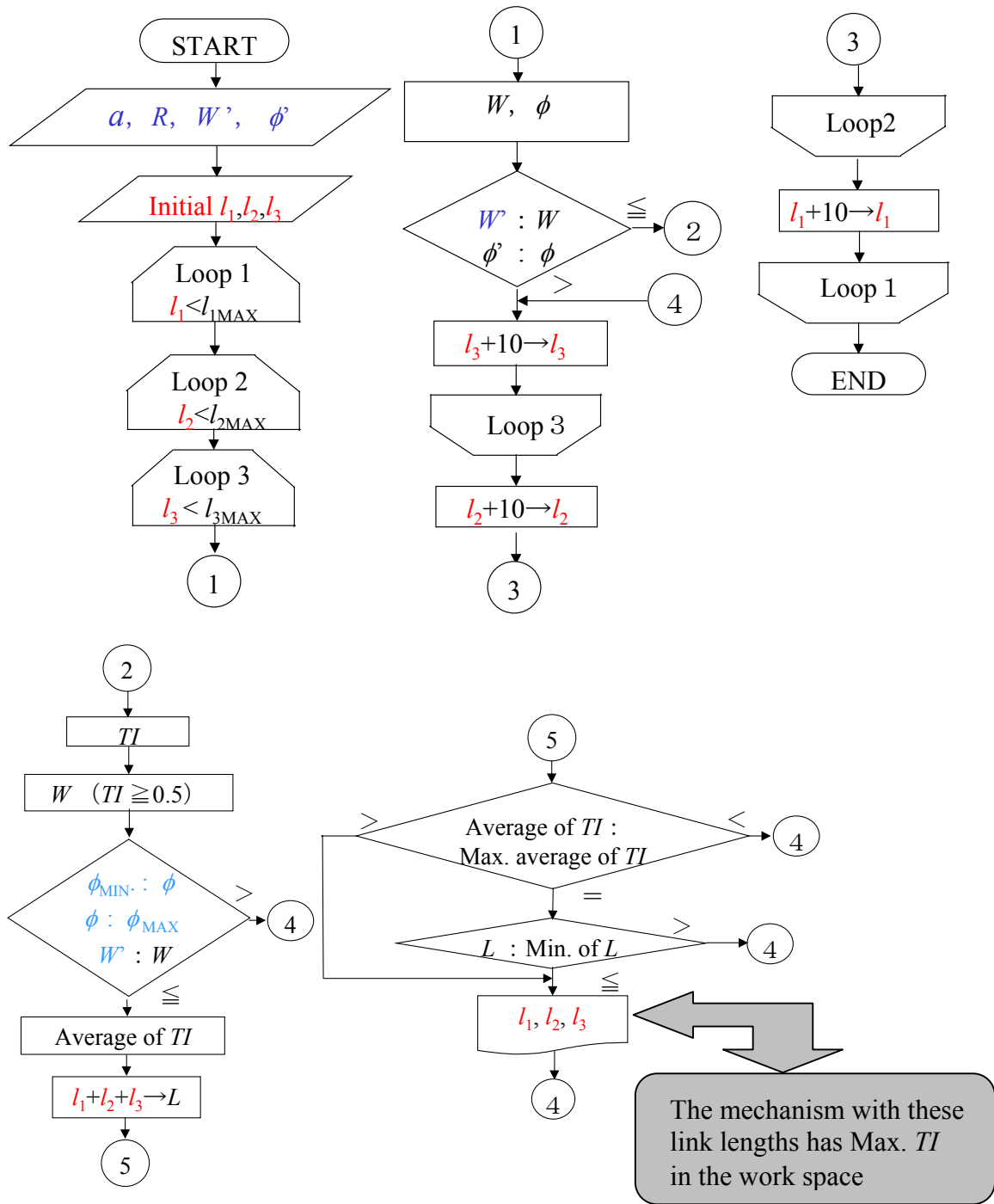


Fig. 10 Design flowchart of 3-DOF parallel mechanism with large-deflective hinges

Table 1 Specification of table parameters

Representative length of output link a (mm)	40
Y direction length in work space W (mm)	50
Distance between two rails R (mm)	100
Minimum orientation angle ϕ min.(deg.)	-10
Maximum orientation angle ϕ max.(deg.)	+10

Table 2 Design results

l_1 (mm)	140	TI	Min.	0.68
l_2 (mm)	90		Max.	0.99
l_3 (mm)	90		Average	0.93

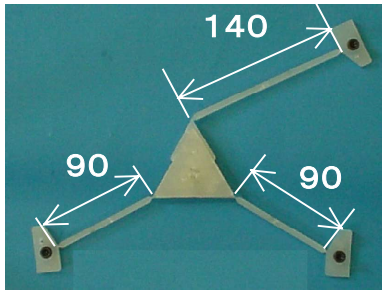
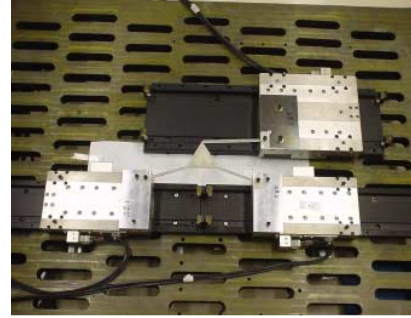


Fig. 11 Manufactured 3-DOF table with large-deflective hinges and links (Unit : mm)



(a) Experimental apparatus to find the singular points of the proposed 3-DOF parallel manipulator with three linear actuators

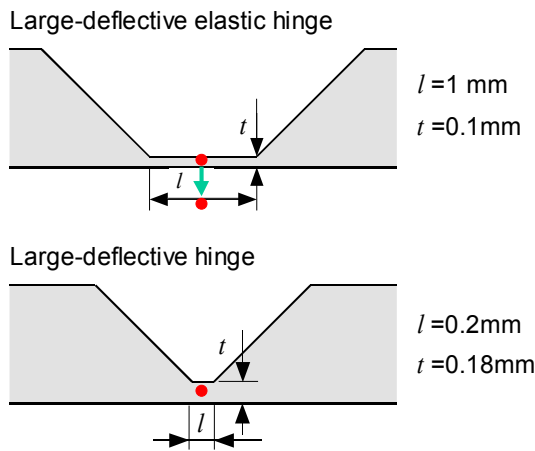
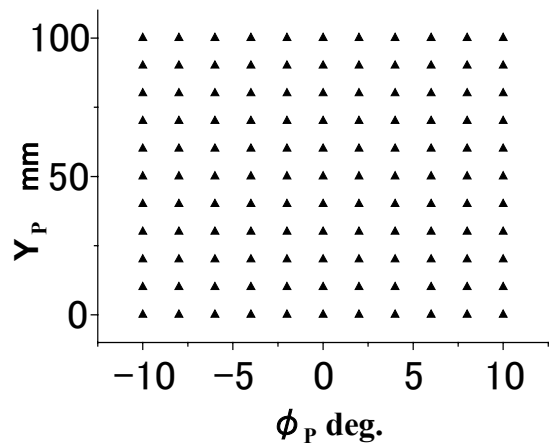


Fig. 12 Hinge center points (Red circles) of large-deflective elastic hinge and large-deflective hinge

injection-molding machine. Figure 12 shows the enlargement hinge shape. In case of large-deflective elastic hinge in upper part of Fig. 12, when links move, the center point of the hinge moves largely. However, in case of a large-deflective hinge in lower part of Fig. 12, the center point of the hinge does not move largely, when links move. Therefore, it is possible to obtain the small output error mechanism in case of large-deflective hinge in lower part of Fig. 12.

As shown in Fig. 13 (a), linear actuators were connected on three sliding parts of this table. Then the existing space of singular points were examined in the positioning-orientation table actually manufactured. The method is as follows: examining whether the manufactured table could be movable from 100 points within the space of $Y_p = 0 \sim 100 \text{ mm}$ and $\phi_p = -10 \sim 10 \text{ (deg.)}$, the experiment confirmed there was no existing singular points as shown in Fig. 13 (b).



(b) Results of existing space of the singular points (▲ : No existence of the singular points)

Fig. 13 Experiments concerning singular points investigation

6. Conclusion

After the existing space of the singular points in the mechanism composed of hinges was examined, the result was examined and compared with the theoretical results. This study confirmed the method for obtaining transmission indexes of the suggested mechanism composed of hinges as well as the effectiveness of the mechanism.

Acknowledgments

This study is partially supported by the Scientific Research Grant-in-Aid No.13555040 from the Japan Society for the Promotion of Science.

References

1. Mikio HORIE and Daiki KAMIYA : A Pantograph Mechanism with Large-deflective Hinges for Miniature Surface Mount Systems ; Book of Abstracts(Thirteenth CISM-IFToMM Symposium on the Theory and Practice of Robots and Manipulators), p. 10, 2000.

Adhesion of RF Bias-Sputtered Cr Thin Films onto Photosensitive Polyimide Substrates

Sun Young Kim, Young-Ho Kim, and C. S. Yoon

Department of Materials Engineering, Hanyang University, Seoul, 133-179, Korea
istine77@hotmail.com phone: 82-2-2290-0405 fax: 82-2-2293-7445

Abstract

The adhesion enhancement from inserting a RF bias-sputtered Cr layer between Cu and polyimide (PI) has been studied. The RF bias power applied in this study was ranged from 0 to 400 W. Without the RF bias, the peel strength, which measures the adhesion strength, was nearly 0 g/mm. As the RF power was increased, the peel strength rose up to ~130 g/mm at 200 W, which remained constant with further increase of the RF bias power. Cross-sectional transmission electron microscopy(TEM) was used to investigate the interfacial reaction between the Cr film and PI substrate during the bias sputtering. The Cr/PI interface without the application of RF bias showed a clean, sharp interface while the RF biased Cr/PI interface had about 10~30 nm thick atomistically mixed interlayer between the metal film and PI substrate. This interlayer appeared to have resulted from the implantation of high energy adatoms during the RF bias sputtering of Cr film. This mixed layer serves as an interlocking layer, which enhances adhesion between the metal and PI layers.

1. Introduction

Recently, polyimide (PI) has been used for dielectrics and passivation layers in MCM devices and wafer level packaging due to its excellent thermal stability, low dielectric constant, and chemical inertness.[1,2] However, adhesion properties between Cu and PI is very poor that, in spite of the potential, the polyimide film has not been widely used because of the difficulties involved with adhesion of Cu with PI.[3] To enhance the Cu/PI adhesion, various techniques have been developed. One of these attempts includes the insertion of the adhesion layer between Cu and PI. Previous studies showed that DC sputtered Cr, Ta, Al adhesion layer between Cu and PI layers produced better adhesion properties than those of Cu/PI films without the adhesion layer [4-6]. In a recent study, Ag was sputtered with DC bias onto the polyester substrate to enhance the adhesion characteristics. The sputtering with DC bias accelerates the sputtered adatoms towards the substrate and imparts extra kinetic energy to the adatoms in order to enhance the adhesion of the atoms to the substrate. In the experiment, the polyester substrate was thin enough that the DC bias could be applied to a non-conductive surface.[7]

Although it was demonstrated that the adhesion strength of the Cu/Cr/PI can be improved substantially compared to the samples with no adhesion layer between Cu and PI, the adhesion strength for the Cu/Cr/PI will decrease substantially in the following annealing process, which prevents the integration of the metallization of semiconductor device and electro-packaging processes.[8]

To resist the adhesion degradation after heat treatment, as well as to further increase the adhesion strength, sputtering with RF bias was introduced in our research. The RF bias sputtering produces good adhesion characteristics to the substrate and uniformity in the thin film quality. In addition, the bias sputtering has further benefits of good coverage and substrate heating effect due to the bombardment of the accelerated adatoms and also brings the possibility of in-situ cleaning prior to the deposition. The process can be applied to non-conductive surfaces without any restrictions in the thickness of the dielectric film. In spite of such advantages of the RF bias during sputter deposition, the effects of the RF bias sputtering on the adhesion of Cu/Cr/PI has not been well studied.

In this study, we have characterized the adhesion behavior of Cu/Cr/PI system while the RF bias power was altered during the deposition of Cr adhesion layer on PI substrate. Cross-sectional transmission electron microscope (TEM) is used to study the adhesion mechanism of the Cr film onto the PI substrate.

2. Experimental

The polymeric material used in this study was imidized from the polyamic solution commercially available from Toray under the trade name BG2480. The films of the polyimide were obtained by spinning the polyamic acid precursor diluted in N-methyl-pyrrolidone(NMP) onto silicon wafer. After the coating, all samples were baked at 60 °C for 50 minutes in a convection oven to remove most of the NMP solvent. Subsequent curing steps were carried out under a nitrogen curing ambient at 150 °C for 30 minutes and 350 °C for 3 h. Higher temperature steps are required to remove the remaining solvent and to thermally dehydrate the amic acid group to create the imide film. All films prepared are approximately 6 μm in thickness..

Cr and Cu were deposited onto the polyimide films using magnetron-sputtering system. The base pressure was 1.2×10^{-6} torr and processing pressure was 0.67 Pa (5 mtorr). Cr was deposited with RF bias sputtering whose power ranged from 0 W to 400W and the thickness of Cr adhesion layer was 50 nm. The Cu layer (500 nm) is then deposited by DC sputtering on top of the Cr layer. For the peel test, the thin film stack was deposited through a metal mask with 2 mm wide line patterns and 20 μm-thick Cu was electroplated on Cu/Cr/PI using CuSO₄ solution.

The adhesion strength was evaluated by using a 90 peel test. A schematic diagram of the peel test fixture using a tensile test machine is shown in Figure 1. The test specimen was loaded into a designed specimen holder with the end of a strip attached to a high-sensitivity load cell. The metal film was stripped at a constant rate of 2 mm/min. As the film is

peeled off, the specimen holder moves horizontally, thus it is possible to perform the peeling action while maintain the the angle at 90 degree to the substrate. The force needed to peel off thin films was recorded and converted to the peel strength (peel force/strip width).

In order to elucidate the interfacial microstructures between Cr and PI, we have used cross-sectionanl TEM analysis (model JEOL2010 operating at 200 KeV). To prepare the cross-sectional TEM specimen, the specimen is mounted and sliced using precision diamond saw. The speciemn is ground to 10~20 μm in thickness and ion milled at room temperature until the sample is electron-transparent.

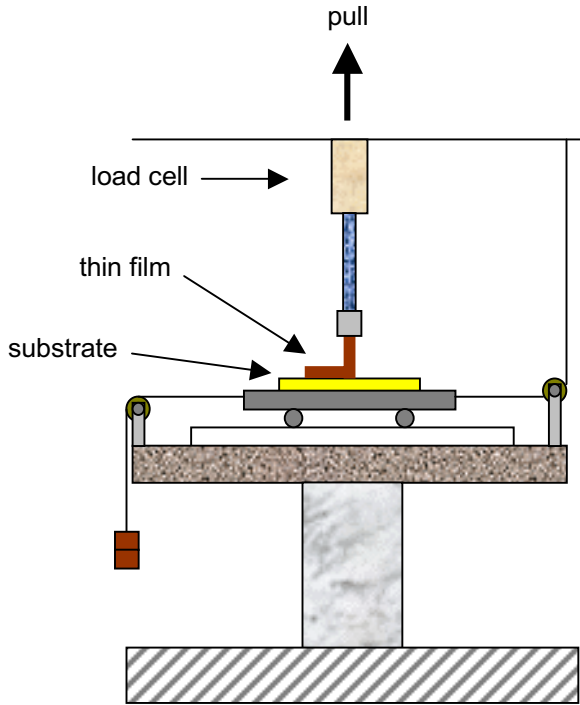


Figure 1. Schematic diagram of peel test fixture

3. Result

The relationship between the RF bias power during deposition of the Cr layer and the measured peel strength of Cu/Cr layer on PI is shown in Figure 2. As can be seen in Figure 2, the peel strength was very low at ~ 0 g/mm for the Cr film without the RF bias; however, the peel strength increased as the RF bias power was raised to 100 W. The peel strength increased further until it reached a saturation point, which was around 200 W.

The peel strength obtained using the RF bias sputtering above 200W is actually larger than that obtained after the RF cleaning treatment. The RF bias-sputtering method is very effective in enhancing the adhesion of Cr onto the PI substrate. A similar conclusion was reached when the adhesion layer of Ta, Al, Ti was sputter-deposited with RF bias. [8,11]

Since the adhesion properties largely depend on the microstructures of interface, the interface between the Cr metal film and PI was observed using cross-sectional TEM to

better understand reasons for the observed adhesion enhancement. Figure 3 shows the cross-sectional TEM images of the interface between Cr and PI layers when the Cr film was deposited with DC sputtering method.

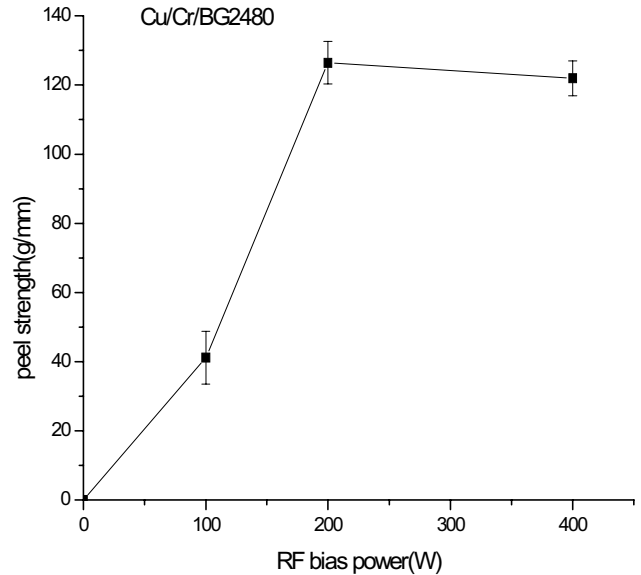


Figure 2. Plot of the peel strength of the Cr/Cu strip on the polyimide substrate versus RF bias power applied during the Cr deposition.

As can be seen in Figure 3 (a), the Cr grains had columnar structure and the interface between Cr and PI is very flat, clean. As shown in dark field image in Figure 3 (b), no reaction interlayer was found between the Cr film and the PI substrate. The TEM observation that no reaction layer exists at the Cr/PI interface with DC sputtering is in agreement with other researchers. [10]

Figure 4 shows cross-sectional TEM images of Cr/PI interface, when the Cr layer was deposited with the RF bias at 100W. Figure 4 reveals that the interface was not sharp compared with that of Figure 3 and it can be seen that there is ~ 10 nm thick interlayer between the Cr grains and PI substrate as indicated in Figure 4.

Figures 5 and 6 show the cross-sectional TEM images of Cr and polyimide interface when the RF power of bias sputtering was at 200W and 400W respectively. In Figures 5 and 6, the mixing layer also exists in polyimide region at the interface and this mixing layer at 200W and 400W (15~30 nm thick) were thicker than that of the 100W sample. This mixing layer seems to have formed not by chemical reaction of Cr with polyimide but by implantation of Cr itself to the polyimide substrate. The interlayer is not a product of interfacial reaction such as oxidized or carbonized phase as confirmed with microbeam electron diffraction, but it is a compositionally

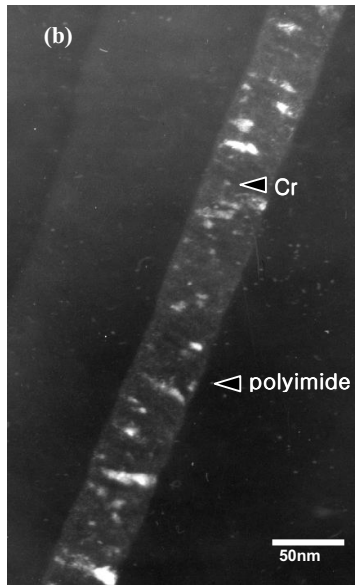
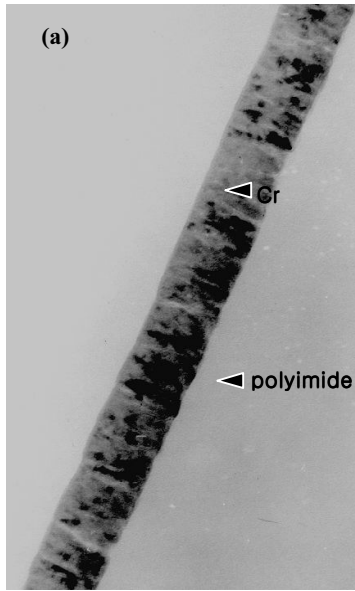


Figure 3. Transmission electron micrographs of DC sputtered Cr/ polyimide (a) Bright-field image (b) Dark-field image

mixed layer created by implantation process during sputtering. Such mixed layer serves as an interlocking layer, which can explain the improved adhesion strength at RF bias power of 200W, 400W samples compared to the sample without the RF bias.

The dark field images of Cr layer, in Figures 4(b), 5(b), and 6(b), also show that Cr grain structure has changed as the RF bias power of the Cr layer was increased. When the RF bias power of Cr layer was at 100W (Figure 4(b)), the Cr film was composed of equiaxed grains. The Cr grains were of intermediate form between columnar and equiaxed structure at 200W (Figure 5(b)) and eventually, the Cr film became perfect columnar at 400W(Figure 6(b)).

Therefore, the bias power not only affects the adhesion process at the Cr/PI interface, but also alters the growth morphology of the Cr film as the film tended to grow columnar as the bias power is increased.

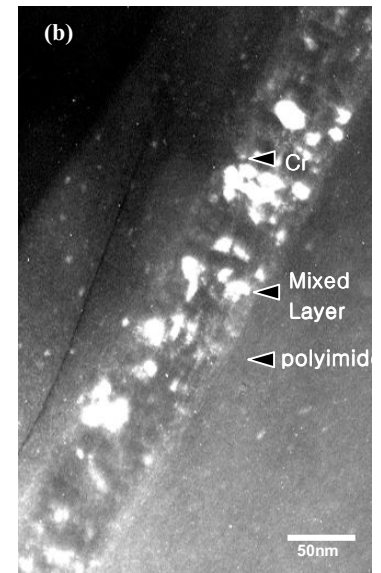
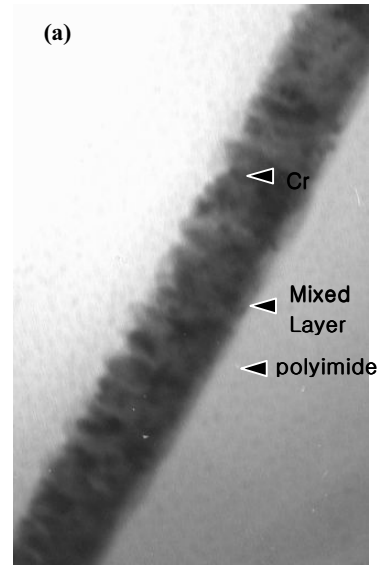


Figure 4. Transmission electron micrographs of RF bias sputtered (100W) Cr/ polyimide (a) Bright-field image (b) dark-field image

The temperature of substrate will typically rise up to 400 °C when the RF bias is applied to substrate [10]. The mixing layer which is found at the bias power of 200W and 400W could have been formed not because of the implantation effect, but because of the solid state diffusion induced by the substrate heating effect of the RF bias sputtering. To study the effect of the substrate heating due to the RF bias, as illustrated in Fig. 7, an initial layer of 50 nm thick Cr is deposited on the PI substrate with no RF bias, after which another layer of Cr film is applied with the 400W RF bias. TEM image of the Cr/PI interface is shown in Figure 8. The Cr/PI interface was clean compared to the interfaces in Figures 5 and 6, which suggests that the direct heating effect of the RF bias would not produce such a mixing layer as observed in Figures 5 and 6.

We have also sputtered the Cr layer on the PI substrate

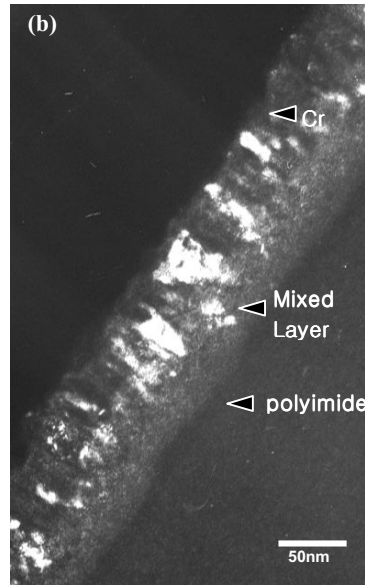
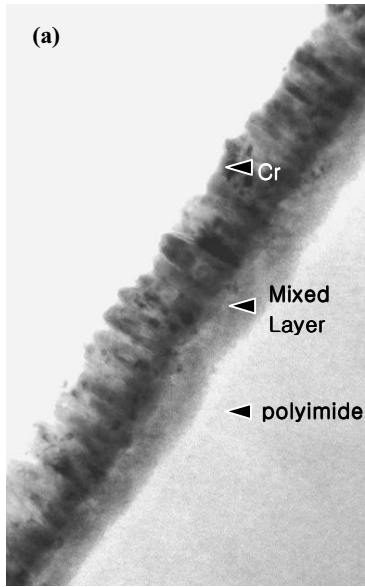


Figure 5. Transmission electron micrographs of RF bias sputtered(200W) Cr/ polyimide (a) Bright-field image (b) dark-field image

without the RF bias, as described in Figure 8, while the substrate is thermally heated to 400 °C. The interface between the PI substrate and the Cr film without the RF bias was again observed to be free of the mixed interlayer as can be seen from the TEM images in Figure 9. From the two sets of experiment, it can be concluded that the mixed interlayer is created by the implantation effect of the RF bias.

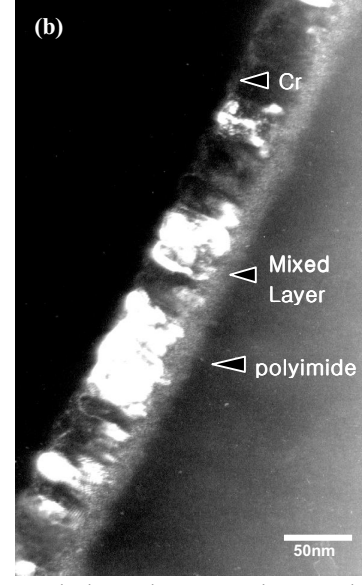
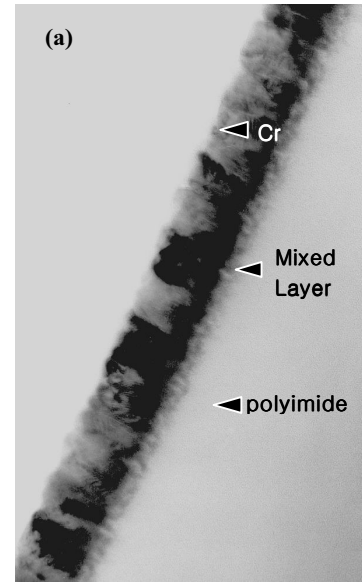


Figure 6 Transmission electron micrographs of RF bias sputtered(400W) Cr/ polyimide (a) Bright-field image (b) dark-field image

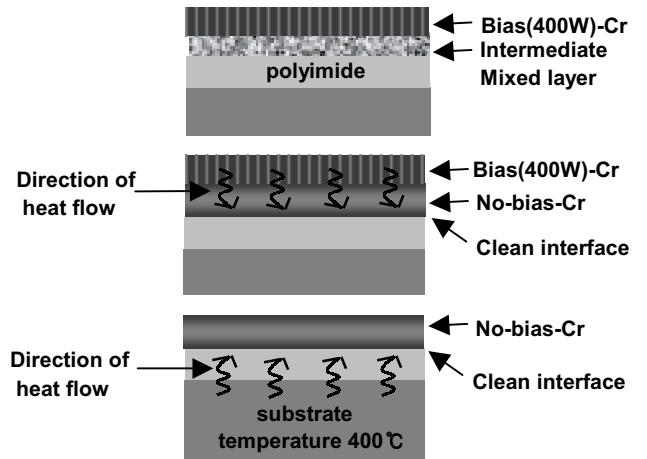


Figure 7 Schematic drawing of the deposited film stack to test the heating effect on the Cr/PI interface.

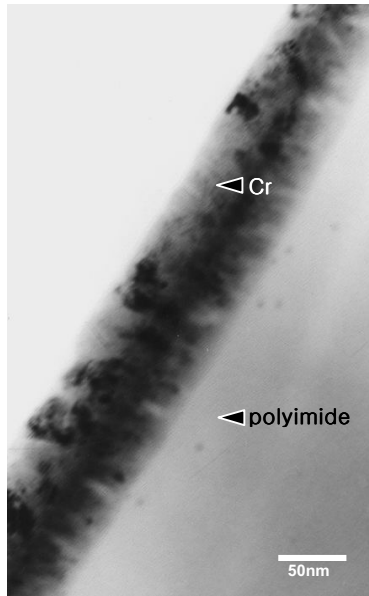


Figure 8 The TEM bright-field image of the film stack consisting of Cr sputtered with RF bias at 400W / Cr without the RF bias / PI.

4. Discussion

The RF bias sputtering combines the DC sputtering of the target for deposition with the RF sputtering of the substrate so that the substrate can be in-situ RF sputter-cleaned. At the same time, the RF plasma above the substrate induces strong ion bombardment of adatoms towards the substrate. The adatoms arrive at the substrate with higher kinetic energy when the RF bias is applied, which, in turn, leads to adhesion enhancement between the metal atoms and the non-conductive substrate surface. The surface of substrate is chemically activated by the accelerated ions which promotes strong bonding of the adatoms to the substrate

As the accelerated adatoms are implanted into the substrate, a compositionally mixed interlayer is produced at the interface of two films so that two layers can adhere to each other through the interlocking effect of the mixed interlayer. The adhesion enhancement or the peel strength does not appear to depend on the thickness of mixed layer once the interlayer is developed since the increase of the peel strength levels out above 200W and the cohesive fracture was observed to occur above RF bias power of 200 W [8,11]. The interfacial strength enhanced through the mixed interlayer is strong enough that the fracture proceeds through the bulk of PI, not through interface of the Cr/PI when the bias power was above 200 W. The superior peel strength can be attributed to the thick mixed interlayer that can be seen in Figures 5 and 6.

Conclusions

According to our observations, an atomistically mixed interlayer generated by the RF bias sputtering can improve the adherence of the Cr film to the polyimide substrate. The improved adhesion strength is originated from the thick mixing layer created at the interface of Cr/PI by the

implantation effect of the RF bias. We suggest that creating a compositionally gradient layer between Cr and PI to physically lock the Cr and PI is the key to strengthening the interfacial bonding.

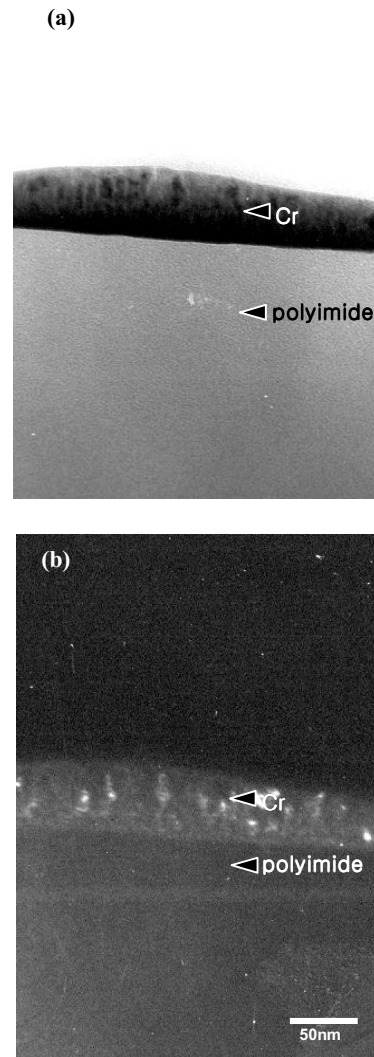


Figure 9 TEM images of the Cr film without the RF bias/ PI interface while the substrate is maintained at 400 °C: (a) Bright-field image (b) dark-field image.

Acknowledgments

This work was supported by Center for Electronic Packaging Materials of Korea Science and Engineering Foundation.

References

1. R. R. Tummala and E. J. Rymaszewski (Eds), "Microelectronics Packaging Handbook." Van Nostrand Reinhold, New York(1989)
2. M. K. Ghosh, K. L. Mittal(Eds), "POLYIMIDES" Marcel Dekker, New York(1996)
3. B. K. Furman, K. D. Childs, et al, J. Vac. Sci. Technol. A10(4), Jul/Aug 1992[1]

4. M. Stravrev, D. Fischer, C. Wenzel, K. Drescher, N. Mattern, *Thin Solid Films* 307, 79-88(1997)
5. K. H. Min, K. C. Chun, and K. B. Kim, *J. Vac. Sci. Technol. B* 14(5) (1996)
6. C. H. F. Peden, K. B. Kidd, et al, *J. Vac. Sci. Technol. A*9(3), May/Jun 1991[2]
7. Ri Eui Jae *J. Kor. Met. & Mater.* Vol. 37, No. 8(1999)
8. J.-S. Kang, MD thesis, Hanyang Univ. (2000)
9. D. C. Kim, C. H. Cho, Y. H. Kim, Korean Institute of Metals and Materials, Poster presentation, (1997)
10. D. M. Mattox, *J. Vac. Sci. Technol. A*7(3), May/Jun 1989[9]
11. J.-G. Jung, MD thesis, Hanyang Univ. (2000)